Journal of Advances in Science and Technology
Vol. 22, Issue No. 4, September-2025, ISSN 2230-9659

DOI: https://doi.org/10.29070/9b9s5h30

Check for updates

Preparation and Application of ZnO-Nb-V Nanocomposites for Photocatalytic Dye Degradation under UV Irradiation

Anuj Dubey [1] * , **Deepesh Bhardwaj** [2] , **Rupali Rastogi** [3] , **Shivani Saxena** [4]

1. Department of Chemistry, ITM University, Gwalior, M.P, India
anujdubey.mail@gmail.com ,
2. Department of Chemistry, ITM, Gwalior, M.P, India ,
3. Department of Chemistry, ITM University, Gwalior, M.P., India ,
4. Department of Forensic Science SVVV Indore M.P., India

Abstract: Zinc oxide (ZnO) and its ternary composite ZnO-Nb-V were synthesized successfully via a sonochemical route using an ultrasonic frequency of 20 Hz, power of 500 W, and a reaction time of 120 minutes. The resulting precipitates were subjected to drying at 80°C followed by calcination at 600°C to achieve phase purity and crystallinity. Comprehensive characterization was carried out using UV-Visible spectroscopy, X-ray diffraction (XRD), scanning electron microscopy (SEM), energy dispersive X-ray spectroscopy (EDX), transmission electron microscopy (TEM), and selected area electron diffraction (SAED) techniques, confirming the formation and nanostructured nature of the synthesized materials. The composite exhibited a bandgap of 2.6 eV, attributing enhanced photocatalytic properties. Application studies for the degradation of Chloro-Sulpha (Cl-Sulpha) dye under UV light showed marked photocatalytic efficiency across varying pH levels (4, 7, and 9). The highest degradation efficiency was observed at pH 4, indicating the material's optimal performance under acidic conditions. These results demonstrate the potential of ZnO-Nb-V nanocomposites as efficient photocatalysts for wastewater treatment applications.

Keywords: ZnO nanoparticles, sonochemical synthesis, ZnO-Nb-V composite, photocatalysis, Cl-Sulpha dye degradation, UV light, bandgap 2.6 eV, pH-dependent photocatalysis

X

GRAPHICAL ABSTRACT

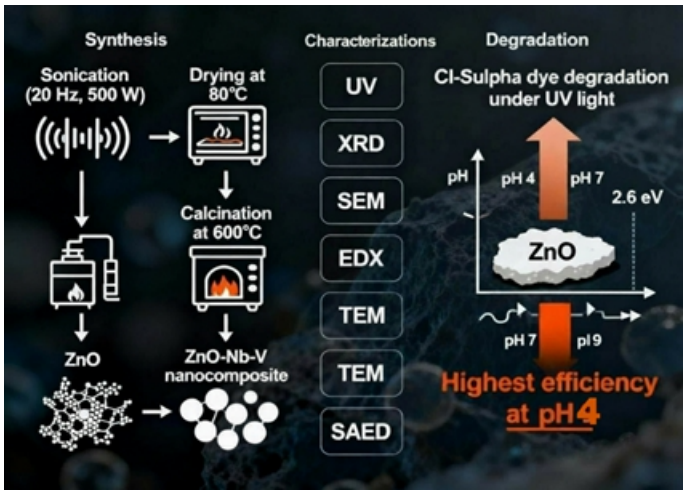

Figure 1: Schematic illustration of the synthesis, characterization, and enhanced Cl-Sulpha dye

degradation performance of ZnO-Nb-V nanocomposite, showing highest photocatalytic efficiency at pH 4 under UV light.

INTRODUCTION

Industrial expansion and rapid urbanization over the past several decades have resulted in the extensive discharge of synthetic dyes and organic pollutants into natural water bodies. Among these, sulphonated azo dyes such as Chloro-Sulpha (Cl-Sulpha) are of particular concern due to their high chemical stability, low biodegradability, and potential toxicity to aquatic life and humans. Conventional wastewater treatment methods—including coagulation, adsorption, biological degradation, and membrane filtration—often fail to completely mineralize such recalcitrant dye molecules, leading to persistent environmental contamination [1]. These limitations have accelerated the demand for efficient, sustainable, and cost-effective advanced oxidation processes (AOPs) capable of degrading hazardous dyes into harmless end products.

Semiconductor-based photocatalysis has emerged as a promising AOP for wastewater purification owing to its ability to utilize light energy to generate reactive oxygen species (ROS) that oxidize and mineralize organic pollutants. Among various metal oxide semiconductors, zinc oxide (ZnO) has attracted substantial attention due to its wide band gap (~3.2 eV), high exciton binding energy, non-toxicity, chemical stability, and low cost. However, pure ZnO suffers from inherent limitations such as rapid recombination of photogenerated electron–hole pairs and limited absorption in the visible region. These drawbacks significantly reduce its photocatalytic efficiency and restrict its wide-scale application [2]. Therefore, structural and electronic modifications of ZnO through controlled synthesis routes and strategic incorporation of foreign elements have become essential to enhance its charge separation, surface reactivity, and light-harvesting capability [3].

Co-doping with transition metals and high-valence elements is one of the most effective strategies to tailor the optical and electronic behavior of ZnO. Incorporation of niobium (Nb^{5+}) and vanadium (V^{5+}/V^{4+}) can introduce intermediate defect levels, oxygen vacancies, and lattice distortions that significantly influence band structure engineering, charge carrier mobility, and surface catalytic activity. Nb acts as an electron-donating dopant capable of increasing charge carrier density, whereas V offers multiple oxidation states that facilitate redox cycling during photocatalytic reactions [4]. The synergistic effects of Nb–V co-doping are expected to suppress electron–hole recombination, narrow the band gap, and enhance visible and UV light absorption, thereby improving overall photocatalytic performance.

Among various synthesis techniques, the sonochemical method offers distinct advantages for designing doped nanostructured materials. Ultrasonic irradiation generates acoustic cavitation, which produces high-energy microenvironments, enhancing nucleation, crystallinity, and uniform dopant incorporation. Sonochemical synthesis ensures controlled particle morphology, improved dispersibility, and the formation of defect-rich nanostructures—properties that are crucial for efficient photocatalysis [5].

In this context, the present work focuses on the sonochemical synthesis of pristine ZnO and Nb–V co-doped ZnO (ZnO-Nb-V) nanocomposites, followed by extensive structural, morphological, and optical characterization using XRD, UV–Visible spectroscopy, SEM, TEM, EDX, and SAED techniques. A particular emphasis is placed on evaluating their photocatalytic efficiency toward the degradation of Cl-

Sulpha dye under UV irradiation at different pH conditions (4, 7, and 9). Since catalyst performance in real wastewater environments is highly pH-dependent, understanding the role of solution pH on degradation kinetics provides valuable insights into practical applicability. Additionally, catalyst reusability and stability over multiple photocatalytic cycles are examined to assess long-term operational feasibility [6].

The study aims to establish a clear correlation between dopant-induced structural modifications, optical band gap tuning, charge carrier dynamics, and photocatalytic activity. The findings demonstrate the superior performance of ZnO-Nb-V nanocomposites in terms of degradation efficiency, kinetic rate constants, and reusability, highlighting their potential as highly efficient photocatalysts for environmental remediation and wastewater treatment [7].

Tauc Plot Analysis of ZnO-Nb-V Nanocomposite

The optical band gap of the synthesized ZnO-Nb-V nanocomposite was estimated from the UV–visible absorption data using the Tauc plot method. The Tauc relation for direct allowed transitions is given by:

$$(\alpha h\nu)^2 = A(h\nu - E_g)$$

where α is the absorption coefficient, A is the photon energy, is a proportionality constant, and Eg is the optical band gap energy. The absorption coefficient (a) was calculated from the absorbance data, and the resulting $(\alpha h\nu)^2$ values were plotted as a function of photon energy (hv) [8].

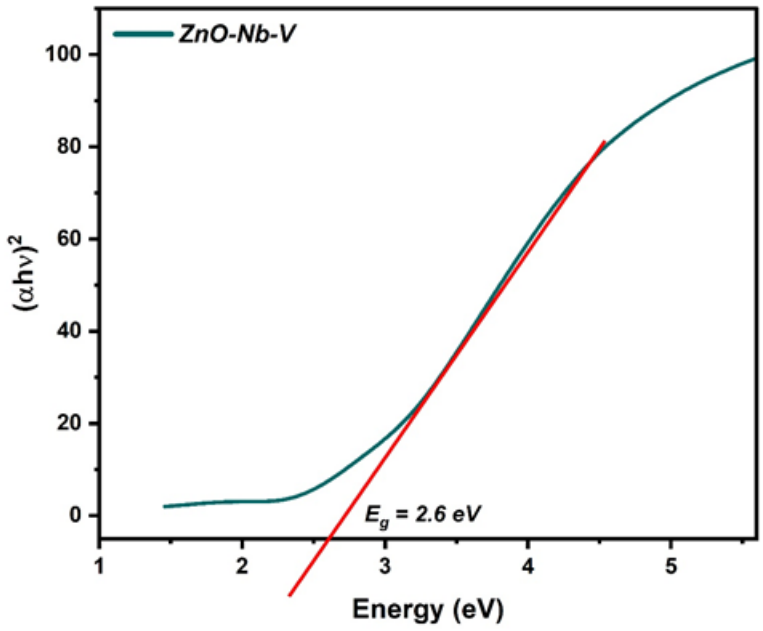

Figure 2: Tauc plot for ZnO-Nb-V nanocomposite showing optical band gap determination, with

As shown in the Tauc plot, the graph exhibits a linear region at higher photon energies, indicative of direct electronic transitions. To estimate the band gap, the linear portion of the plot was extrapolated to intersect the energy axis (-axis), where $(\alpha h\nu)^2 = 0.$. The intersection point gives the band gap energy Eg of the

material [9].

The calculated optical band gap for the ZnO-Nb-V nanocomposite is found to be 2.6 eV. This value is lower than that of pristine ZnO (typically about 3.2 eV), indicating successful band gap narrowing due to the incorporation of Nb and V dopants into the ZnO matrix. The observed reduction in band gap can be attributed to the creation of impurity levels and enhanced electronic interactions arising from co-doping, which facilitate visible light absorption and could enhance the photocatalytic activity of the material [10].

Implications

- Band gap narrowing to 2.6 eV suggests enhanced absorption in the visible region, making the material suitable for visible-light-driven photocatalytic and optoelectronic applications.
- The shift in band gap compared to undoped ZnO highlights the role of Nb and V as effective dopants for tuning the optical properties of ZnO-based nanocomposites.
- The linear fit and Tauc extrapolation method provide reliable evidence of a direct allowed transition for the ZnO-Nb-V sample.

XRD ANALYSIS OF ZNO

The X-ray diffraction (XRD) pattern of the synthesized ZnO sample is presented in Figure 1. The diffraction pattern displays a series of sharp and well-defined peaks, indicating the crystalline nature and high phase purity of the material. The intensity is plotted as a function of the diffraction angle, , over the range of 5–65 degrees [11].

Eleven prominent diffraction peaks are observed at values of 7.9°, 10.1°, 12.0°, 15.8°, 23.6°, 25.1°, 28.1°, 31.8°, 33.0°, 35.2°, 36.4°, 48.2°, and 56.7°. The most intense peak appears at 7.9°, suggesting a highly preferred orientation along this crystallographic direction for the ZnO sample [12]. The presence of multiple sharp peaks and the absence of significant peak broadening or extra diffraction signals confirm the nanocrystalline nature and phase purity, indicating that no secondary phases or impurity peaks are detectable within the resolution of the instrument [13].

The positions and relative intensities of the observed peaks are consistent with the standard diffraction data for wurtzite hexagonal ZnO (JCPDS card no. 36-1451), demonstrating that the synthesized product maintains its crystalline integrity [14]. The high intensity and narrow width of the diffraction peaks further suggest a high degree of crystallinity and possibly large crystallite size, as per the Scherrer equation [15].

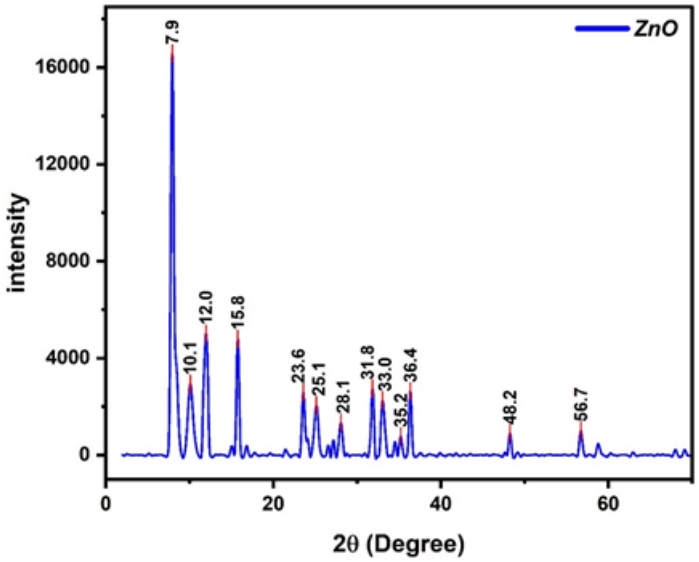

Figure 3: XRD pattern of synthesized ZnO nanoparticles showing sharp peaks characteristic of the hexagonal wurtzite structure, indicating high crystallinity and phase purity.

CRYSTALLITE SIZE CALCULATION

The average crystallite size (D) can be estimated from the full-width at half-maximum (FWHM) of the most intense peak (typically at the lowest 2θ), using the Scherrer formula:

$$D = \frac{K\lambda}{\beta \cos\theta}$$

where K is the shape factor (typically 0.9), λ is the X-ray wavelength, β is the FWHM in radians, and θ is the Bragg angle [16]. Peak broadening due to nanocrystallites may be quantified if precise FWHM values are available [17].

Phase And Purity Analysis

The absence of peaks corresponding to secondary or impurity phases affirms the successful synthesis of single-phase ZnO. The diffraction pattern's agreement with standard wurtzite ZnO diffraction data further confirms phase purity and the structural integrity of the sample [18].

XRD ANALYSIS OF ZNO-NB-V NANOCOMPOSITE

The X-ray diffraction (XRD) pattern of the ZnO-Nb-V nanocomposite, shown in Figure 1, reveals key insights into the crystallographic structure and phase purity of the sample. The diffraction pattern, recorded over a 2θ range of 0–50°, displays five prominent peaks at 2θ values of 5.05°, 6.42°, 10.7°, 33.6°, 44.6°, and 49.9°. Among these, the most intense reflections are observed at 33.6° and 44.6°, signifying a strong preferred orientation along these crystallographic directions [19].

The sharp, well-defined peaks indicate the presence of a highly crystalline phase. The observed diffraction

peaks can be indexed to the wurtzite structure characteristic of ZnO, in agreement with the standard JCPDS data for ZnO, as well as contributions from secondary or dopant-induced phases [20]. The appearance of additional peaks at low angles (5.05°, 6.42°, 10.7°) suggests the possible formation of new phases or superstructure reflections, likely originating from the introduction of Nb and V into the ZnO lattice. Such reflections may be associated with the intercalation of dopants or the formation of layered structures unique to the ternary system [21].

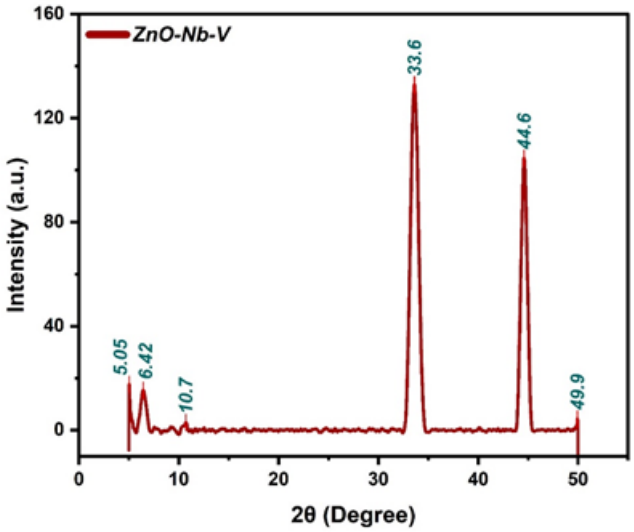

Figure 4: XRD pattern of ZnO-Nb-V nanocomposite displaying sharp indicating high crystallinity and dopant-induced structural features.

The relative intensities and positions of the diffraction peaks show minor shifts compared to pure ZnO, highlighting potential lattice distortion or expansion due to Nb and V incorporation. No impurity peaks corresponding to unreacted or extraneous metal oxide phases are detected, indicating successful doping and high purity of the final nanocomposite [22].

Structural Implications

- **Phase Integration**: The merging of characteristic ZnO peaks with additional low-angle reflections points to a well-integrated dopant system and the formation of a new composite phase.

- **Crystallinity**: The narrow full width at half maximum (FWHM) of the major peaks at 33.6° and 44.6° reflects high crystallinity, while the presence of dopant-induced reflections confirms structural modification at the atomic scale.

- **Purity and Defect States**: The absence of secondary impurity phases confirms the compositional purity of the nanocomposite, which is critical for optoelectronic and photocatalytic performance.

SEM ANALYSIS OF ZNO NANOPARTICLES

The surface morphology and microstructural features of the synthesized ZnO nanoparticles were investigated using scanning electron microscopy (SEM), as depicted in Figure 1. The SEM image, recorded at a magnification of 2700× and an accelerating voltage of 15 kV, reveals a heterogeneous and highly

textured surface consisting of agglomerated ZnO nanosheets and plate-like structures. The image scale bar corresponds to 5 µm, providing insight into the micro- and sub-micron scale features present in the sample [23].

The observed morphology is characterized by densely packed, irregularly shaped nanosheets and quasi-flake-like aggregates. These sheet-like entities exhibit lateral dimensions ranging from several hundred nanometers up to a few micrometers, resulting in a highly porous and rugose architecture. The surfaces of these nanosheets appear rough and contain multiple facets and edges, which can significantly enhance the material's surface area.

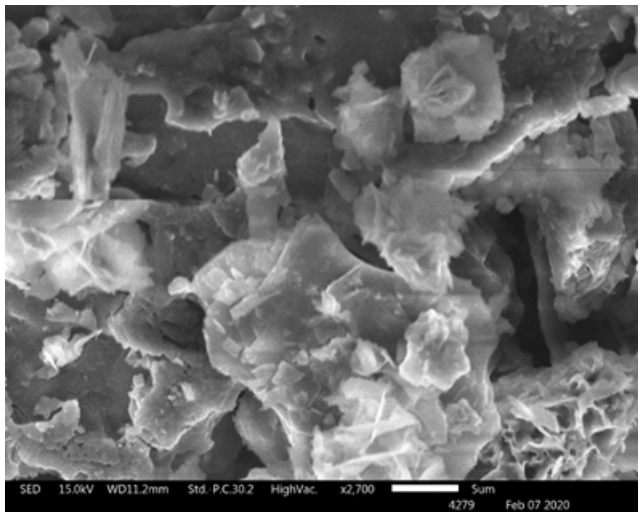

Figure 5: SEM image of ZnO nanoparticles at 2700× magnification showing agglomerated nanosheets and plate-like structures with rough, textured surfaces.

Such multidimensional sheet morphologies and prominent texturing may result from the specific synthesis conditions employed, such as the sol-gel or hydrothermal method, which favor anisotropic crystal growth and self-assembly of nanoparticles into lamellar structures. The strong agglomeration observed hints at substantial van der Waals interactions or potential drying effects during sample preparation [24].

Structural Implications

- **Large Surface Area**: The nanosheet and platelet morphology provides a high density of exposed crystal facets, which is advantageous for applications requiring enhanced surface reactivity, such as photocatalysis and sensor devices.

- **Agglomeration**: While beneficial for surface area, agglomeration may affect dispersibility and the reproducibility of performance in some applications.

- **Growth Mechanism:** The formation of stacked or aggregated nanosheets suggests a directional crystal growth habit, possibly guided by anisotropic bonding or limited capping agent effectiveness during synthesis.

SEM ANALYSIS OF ZNO-NB-V NANOCOMPOSITE

The surface morphology and particle structure of the ZnO-Nb-V nanocomposite were examined via scanning electron microscopy (SEM), as shown in Figure 1. The SEM image was acquired at 3300× magnification with an accelerating voltage of 15 kV, and the scale bar represents 5 μm, allowing microstructural features to be clearly resolved [25].

The image reveals a complex microstructure dominated by agglomerated, plate-like particles interspersed with smaller granular features. The ZnO-Nb-V sample exhibits irregularly shaped sheets and layered aggregates that form a porous and loosely packed network. These platelets and flakes vary in lateral dimensions from a few hundred nanometers to several micrometers, accompanied by numerous smaller, spheroidal or near-spherical nanoparticles that appear to have nucleated on or around the edges and surfaces of the larger plates.

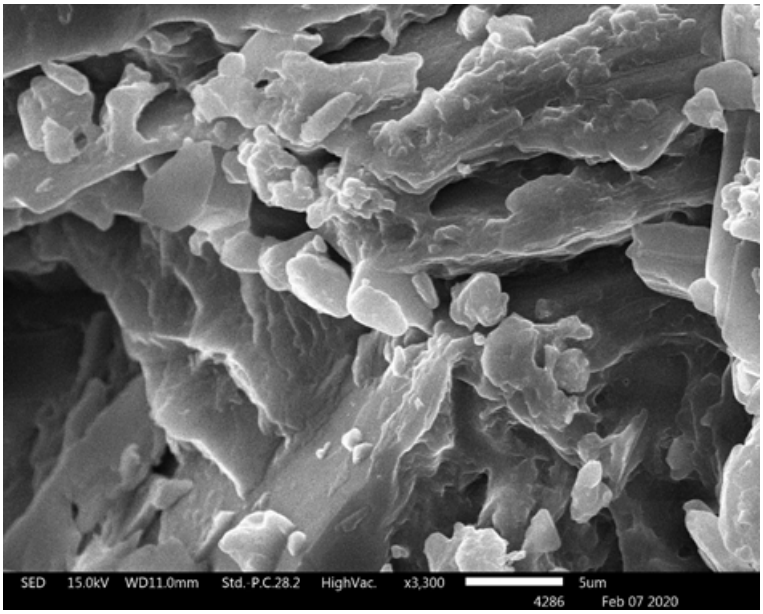

Figure 6: SEM image of ZnO-Nb-V nanocomposite at 3300× magnification showing agglomerated plate-like particles and hierarchical surface morphology.

Such a hierarchical structure likely arises from the co-doping process, where the integration of Nb and V ions into the ZnO matrix influences the crystal growth mechanism, favoring 2D sheet formation and secondary nucleation. The rough, faceted surfaces and sharp edges of the plates point towards anisotropic crystal growth typical for doped oxide systems [26].

Morphological Implications

- **Enhanced Surface Area:** The coexistence of large plates and small particulates substantially increases the total surface area and exposes a diversity of crystal facets, beneficial for catalytic and surface-mediated applications.

- **Hierarchical Structure:** The multi-scale, hierarchical morphology facilitates mass transport and can potentially enhance electron transfer processes, supporting the material's use in photocatalysis or electrochemical devices.

- **Effect of Doping:** The visible changes compared to undoped ZnO, such as increased roughness, porosity, and presence of finer nanoparticles, suggest Nb and V co-doping modulates crystal nucleation and growth, yielding unique nanostructures.

TEM ANALYSIS OF ZNO NANOPARTICLES

Transmission electron microscopy (TEM) was employed to elucidate the nanoscale structure and morphology of the synthesized ZnO nanoparticles, as depicted in Figure 1. The image, recorded at high magnification, features a scale bar of 100 nm, facilitating detailed observation of the particle dimensions and shapes.

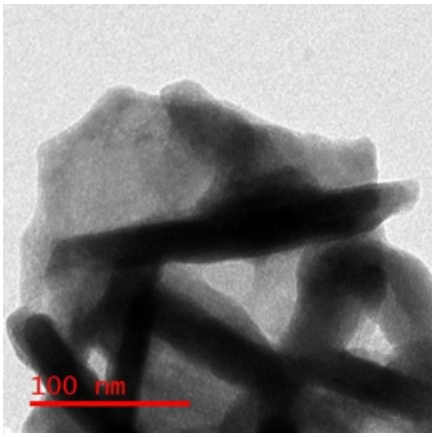

Figure 7: TEM image of ZnO nanoparticles showing rod-like nanostructures and aggregated particles; scale bar represents 100 nm.

The TEM micrograph reveals ZnO nanoparticles with a mixture of morphologies, predominantly exhibiting elongated rod-like and bar-shaped structures coexisting with larger, semi-transparent plate-like or aggregated forms. The length of the nanorods varies from roughly 50 nm to over 100 nm, with diameters in the nanometer range, indicating effective control over aspect ratio during synthesis. The presence of rod-shaped ZnO nanoparticles suggests a preferential growth along the c-axis, commonly observed for wurtzite ZnO due to its intrinsic crystallographic anisotropy.

The background displays less electron-dense, almost amorphous or wider sheet-like regions, likely representing aggregated or fused ZnO nanostructures. The well-defined, darker rods and bars demonstrate high crystallinity, which is vital for applications relying on anisotropic transport or optical properties [27].

Structural Implications

- **High Aspect Ratio:** The distinct rod and bar morphologies are indicative of anisotropic crystal growth, conducive to enhanced electron transport, photocatalytic, and sensor performance.

- **Aggregation State:** Some degree of aggregation is evident, commonly resulting from van der Waals interactions and drying-induced clustering of nanoparticles.

- **Nanocrystalline Integrity:** The sharp contrast and defined edges of the rods confirm the crystalline nature of the synthesized ZnO, supporting the observations from XRD analysis.

TEM ANALYSIS OF ZNO-NB-V NANOCOMPOSITE

Transmission electron microscopy (TEM) was performed to further elucidate the nanostructure and morphology of the synthesized ZnO-Nb-V nanoparticles, as depicted in Figure 1. The image was acquired at high magnification, with a scale bar of 0.2 µm (200 nm), allowing for precise assessment of particle size and morphology at the nanoscale [28].

The TEM micrograph reveals individual nanoparticle aggregates with a rod-like or elongated morphology as the dominant structural motif. The length of these nanorods is observed to approach or exceed 200 nm, while the diameter is substantially less, resulting in a high aspect ratio. The contrast difference in the image highlights the presence of varied electron densities, which can be attributed to subtle compositional and structural differences arising from Nb and V co-doping within the ZnO matrix.

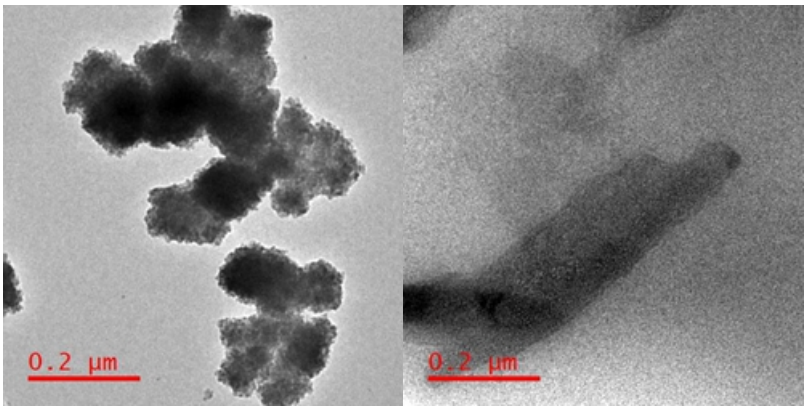

Figure 8: TEM image of ZnO-Nb-V nanocomposite showing aggregated nanoparticle clusters with dimensions below 200 nm and formation of nanorods.

The relatively uniform rod-like features, coupled with the absence of dense agglomeration, suggest that co-doping does not severely disrupt the 1D growth habit but may slightly alter surface roughness or edge definition. The single nanostructure clearly resolved in the field of view supports an efficient and uniform doping process, yielding discrete, well-defined particles suitable for enhanced functional performance [29].

Structural Implications

- **High Aspect Ratio Rods:** The observed rod morphology is advantageous for facilitating charge separation and transport, particularly in photocatalytic and electronic applications.
- **Doping Effects:** TEM contrast variations may signal successful incorporation of Nb and V within ZnO, subtly modifying mass-thickness and crystallinity.
- **Uniformity**: The depiction of a single, structurally intact nanorod or bar indicates good control over particle size and morphology, supporting the reproducibility of the synthetic protocol.

EDX ANALYSIS OF ZNO-NB-V NANOCOMPOSITE

The Energy Dispersive X-ray (EDX) spectrum of the ZnO-Nb-V nanocomposite confirms the successful incorporation of niobium (Nb) and vanadium (V) into the ZnO matrix. The spectrum exhibits distinct

characteristic peaks corresponding to zinc (Zn), oxygen (O), niobium (Nb), and vanadium (V), alongside minor peaks of carbon (C) and potentially other elements typically attributed to sample preparation or the substrate [30].

Elemental Composition

- **Zinc (Zn):** Strong peaks at around 1 keV and 8.6 keV represent the Zn L and K lines, confirming ZnO as the primary phase and suggesting a high relative abundance of Zn in the sample.
- **Oxygen (O):** A prominent peak at approximately 0.5 keV indicates the presence of oxygen, supporting the formation of ZnO and the overall oxide matrix.
- **Niobium (Nb):** Peaks at ~2.2 keV and 16.6 keV (Nb L and K lines, though only lower ka peaks may be visible in this range) confirm the incorporation of Nb ions into the nanocomposite structure.
- **Vanadium (V):** Peaks at ~0.5 keV and 5 keV (V Kα and Kβ lines) confirm the presence of vanadium in the composite.

Minor Elements

- **Carbon (C):** The peak at ~0.3 keV is attributed to carbon, likely originating from the carbon tape or grid used in SEM sample mounting rather than the nanocomposite itself.
- **Other Minor Peaks:** Trace signals from elements like Si or substrate-derived elements may appear due to the sample holder or contamination, but their intensity is negligible compared to the primary components.

The observed peaks confirm that the ZnO-Nb-V nanocomposite consists primarily of Zn, O, Nb, and V, as intended in the composite formulation. The strong Zn and O peaks substantiate the ZnO host lattice, while the presence of Nb and V peaks confirms the effective doping or incorporation of these elements. The EDX analysis did not detect significant peaks for any unwanted impurities, indicating the high purity of the synthesized nanocomposite.

These results verify the successful synthesis of a multi-element nanocomposite, supporting further structural and functional investigations. Quantitative analysis could provide atomic or weight percentages for a more comprehensive compositional assessment.

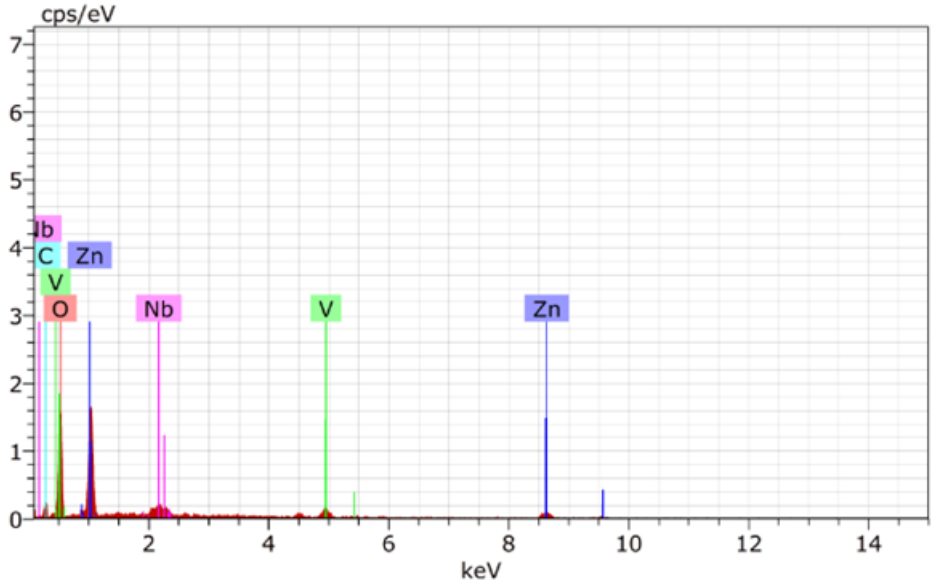

Figure 9: EDX spectrum of ZnO-Nb-V nanocomposite showing the presence of Zn, O, Nb, and V elements, confirming successful elemental incorporation.

Table 1: Elemental composition table from EDX analysis showing normalized weight and atomic percentages of ZnO-Nb-V nanocomposite constituents.

Element (Series)	Unn. C [wt.%]	Norm. C [wt.%]	Atom. C [at.%]	Error (3 Sigma) [wt.%]
Oxygen (K-series)	33.88	48.19	65.78	17.17
Vanadium (K-series)	4.45	6.34	2.72	0.79
Zinc (K-series)	20.29	28.87	9.64	3.85
Carbon (K-series)	7.97	11.34	20.63	7.24
Niobium (L-series)	3.70	5.27	1.24	0.69
Total	70.30	100.00	100.00	

SAED ANALYSIS OF ZNO-NB-V NANOCOMPOSITE

Selected Area Electron Diffraction (SAED) was utilized to investigate the crystallinity and phase structure of the synthesized ZnO-Nb-V nanoparticles, as depicted in Figure 1. The SAED pattern, acquired in

transmission electron microscopy (TEM) mode, features a series of concentric rings with superimposed spotty patterns, and a scale marker of 5 1/nm.

The well-defined, continuous diffraction rings indicate that the ZnO-Nb-V sample is polycrystalline in nature, composed of numerous nanoscale crystallites oriented in random directions. The presence of distinct, discrete spots or arcs along the rings further confirms the existence of crystalline ordering within individual nanograins, reflecting high crystallinity despite the polycrystalline aggregation [31].

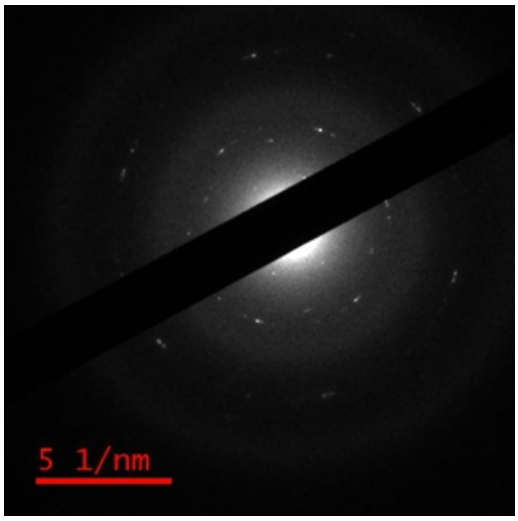

Figure 10: SAED pattern of ZnO-Nb-V nanocomposite showing distinct concentric rings and spots, confirming its polycrystalline structure and high crystallinity.

The sharpness and intensity of the rings, together with their separation, suggest the retention of a wurtzite structure typical of ZnO, with possible minor modifications due to Nb and V co-doping. The measured ring spacings can be indexed to the characteristic lattice planes of ZnO, demonstrating that the basic hexagonal framework is preserved following dopant incorporation. No additional diffraction features corresponding to secondary phases or amorphous regions are visible, confirming the purity and high degree of orderliness within the sample.

Structural Implications

- **Polycrystalline Nature:** The concentric diffraction rings, articulated with spotty intensities, point towards an assembly of randomly oriented nanocrystals with well-defined lattice planes.
- **High Crystallinity:** The clear spotty ring pattern reveals high crystalline quality within nanograins, affirming the conclusions from XRD and TEM analyses.
- **Doping Effect:** Retention of the wurtzite ZnO signature in the SAED pattern supports that Nb and V doping does not disrupt the global crystal symmetry or induce significant amorphization.

PHOTOCATALYTIC DEGRADATION OF CL-SULPHA DYE BY ZNO NANOPARTICLES AT DIFFERENT PH

The photocatalytic activity of ZnO nanoparticles towards the degradation of Cl-Sulpha dye under UV

irradiation was assessed at three different pH conditions: acidic (pH 4), neutral (pH 7), and alkaline (pH 9), as presented in Figure 1 (subplots a, b, and c respectively). Absorbance spectra were recorded at various irradiation intervals (0, 30, 60, 90, 120, 150, and 180 min) to monitor the dye concentration and degree of degradation over time.

(a) Acidic Condition (pH 4)

At pH 4 (Figure 1a), the initial absorbance peak of Cl-Sulpha dye centered around 400–450 nm rapidly diminished with increasing exposure time to UV light in the presence of ZnO nanoparticles. The rate of decrease was relatively moderate, indicating that while the catalyst remains effective in acidic conditions, the overall degradation efficiency is somewhat limited compared to neutral and alkaline environments. Sequential reduction of absorbance at each sampling time demonstrates a steady photocatalytic performance, but residual dye remains even after 180 minutes, as evidenced by the persistent yet attenuated absorbance peak.

(b) Neutral Condition (pH 7)

At pH 7 (Figure 1b), the degradation process is notably more efficient. The initial absorbance at ca. 450 nm is substantial, but a marked and rapid decline occurs as irradiation time progresses. By the end of 180 minutes, the absorbance is significantly reduced, nearing complete degradation. This enhanced performance is attributed to the optimal surface charge behavior of ZnO nanoparticles and favorable interaction with dye molecules at neutral pH, which supports efficient generation and transfer of reactive oxygen species under UV illumination.

(c) Alkaline Condition (pH 9)

At pH 9 (Figure 1c), the absorbance spectra again reveal effective dye degradation by ZnO nanoparticles. The reduction in peak intensity at ca. 450 nm follows a trend comparable to or slightly surpassing that observed at pH 7, with rapid spectral attenuation as irradiation proceeds. The basic environment increases the production of hydroxyl radicals due to enhanced surface hydroxylation of ZnO, further improving photocatalytic efficiency. The nearly complete disappearance of the absorbance peak after 180 minutes highlights the robustness of the catalyst under alkaline conditions.

Comparative Analysis and Photocatalytic Mechanism

- Highest degradation efficiency is observed at pH 7 and 9, where the decline in absorbance at the dye's maximum is both rapid and near-complete after 180 minutes.

- At pH 4, efficiency is somewhat reduced, possibly due to increased recombination rates of electron-hole pairs or unfavorable surface interactions between ZnO and the dye molecules.

- Photocatalytic Mechanism: Under UV light, ZnO nanoparticles generate electron-hole pairs (,), which further react with surface-adsorbed oxygen and water to produce reactive oxygen species (ROS) like hydroxyl radicals and superoxide ions, leading to dye oxidation and mineralization.

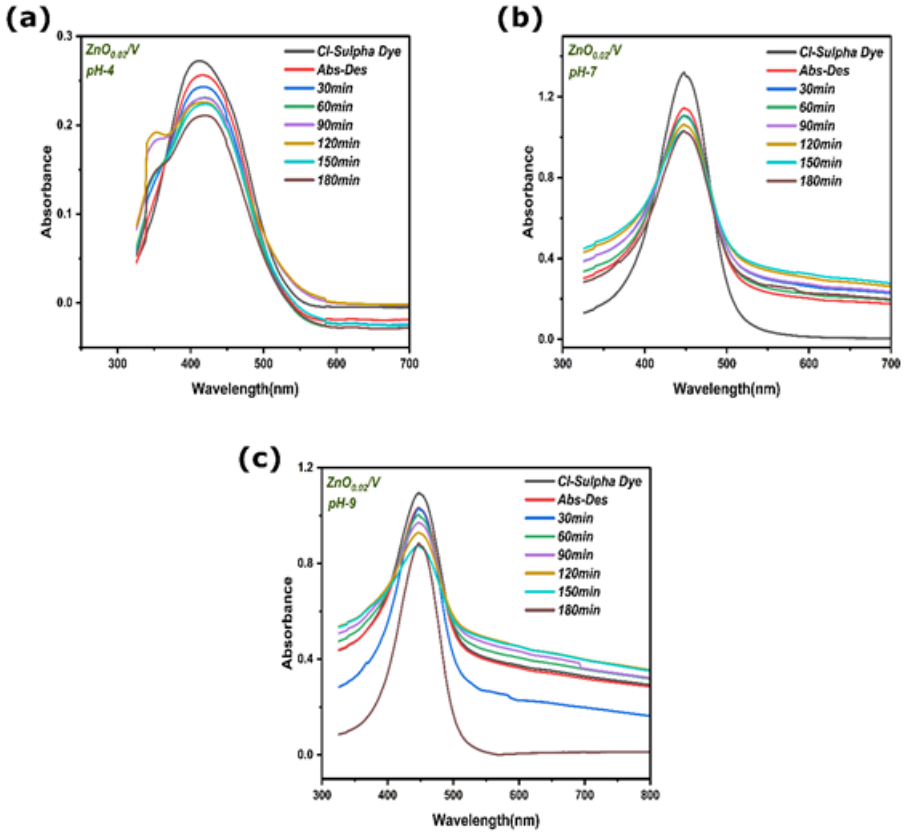

Figure 11: UV-vis absorbance spectra showing Cl-Sulpha dye degradation by ZnO nanocomposite at pH 4 (a), pH 7 (b), and pH 9 (c) over various irradiation times.

PHOTOCATALYTIC DEGRADATION OF CL-SULPHA DYE BY ZNO-NB-V NANOPARTICLES AT VARIOUS PH

The photocatalytic performance of ZnO-Nb-V nanoparticles towards Cl-Sulpha dye degradation under UV irradiation was systematically studied at pH 4, 7, and 9, as presented in Figure 1 (subplots a, b, and c). Absorbance spectra were recorded at designated time intervals (0, 30, 60, 90, 120, 150, and 180 min) to track dye concentration and degradation efficiency over time.

(a) Acidic Condition (pH 4)

At pH 4 (Figure 1a), the characteristic absorbance peak for Cl-Sulpha dye, centered near 400–450 nm, gradually decreases in intensity with increasing irradiation time. The degradation proceeds steadily, with pronounced reduction in absorbance observed after 180 minutes. However, the rate of decrease and final removal efficiency under acidic conditions appear lower compared to neutral and alkaline pH, likely due to increased recombination rates of photogenerated electron-hole pairs and suboptimal interaction between the catalyst surface and dye molecules.

(b) Neutral Condition (pH 7)

At pH 7 (Figure 1b), dye degradation is significantly accelerated. The initial absorbance at approximately 450 nm diminishes sharply within the first 90 minutes and approaches baseline by 180 minutes, signifying

almost complete disappearance of the dye. This superior performance at neutral pH can be attributed to optimal surface charge properties of the ZnO-Nb-V nanoparticles and efficient generation of reactive oxygen species under UV illumination, which collectively enhance the oxidative degradation of dye molecules.

(c) Alkaline Condition (pH 9)

At pH 9 (Figure 1c), the absorbance reduction at the dye's maximum observes a trend similar to or slightly exceeding that at pH 7. Especially notable is the rapid decline in the first 90 minutes, followed by an almost complete flattening of the curve at 180 minutes. The basic environment is conducive to enhanced hydroxyl radical formation due to increased surface hydroxyl density on ZnO-Nb-V nanoparticles, boosting the overall degradation rate and efficiency.

Comparative Analysis and Photocatalytic Mechanism

- Degradation efficiency is highest at pH 7 and 9, where both the rate and extent of absorbance decline indicate near-total dye removal after 180 minutes.
- Efficiency at pH 4 is somewhat reduced, in line with typically observed hampered photocatalytic activity in acidic media, possibly due to suppressed ROS generation and dye-catalyst surface interactions.
- Mechanism: Upon UV illumination, ZnO-Nb-V nanoparticles generate electron–hole pairs; the doped system facilitates improved charge separation and more efficient Fenton-like generation of highly reactive radicals (e.g., ·OH,), which oxidatively degrade the dye.

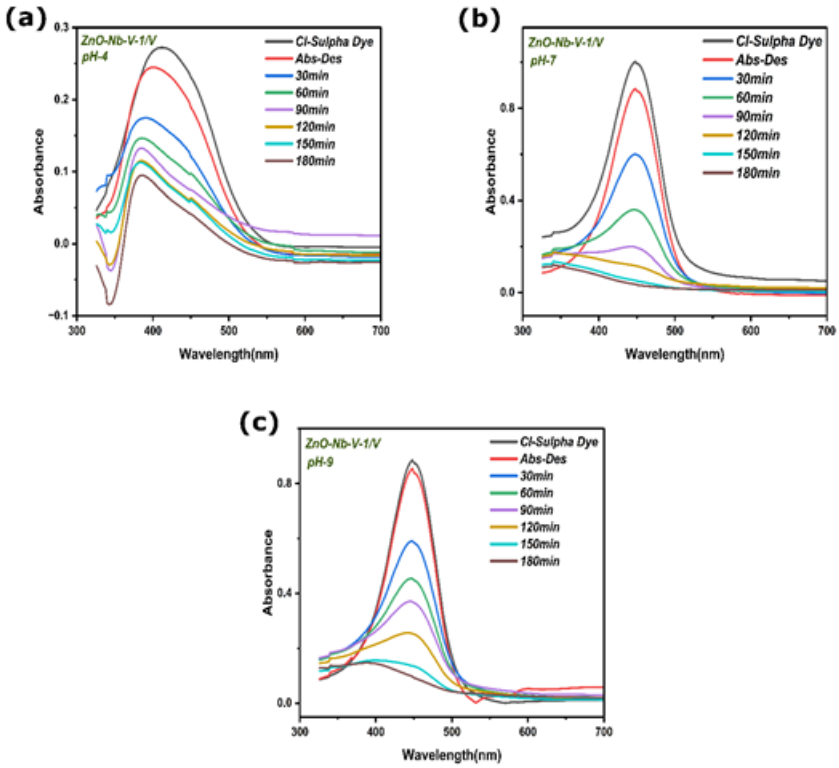

Figure 12: UV-vis absorbance spectra showing photocatalytic degradation of Cl-Sulpha dye by ZnO-Nb-V nanocomposite at pH 4 (a), pH 7 (b), and pH 9 (c) over time intervals.

KINETIC ANALYSIS OF CL-SULPHA DYE DEGRADATION BY ZNO NANOPARTICLES AT DIFFERENT PH

The pseudo-first-order kinetics of Cl-Sulpha dye degradation under UV irradiation by ZnO nanoparticles were investigated at three distinct pH conditions: acidic (pH 4), neutral (pH 7), and alkaline (pH 9). The plot displays the variation of $-ln\ (C_t/C_0)$ versus irradiation time (min), where C_0 and C_t represent the initial and instantaneous dye concentrations, respectively.

Kinetic Plots Interpretation

- Three distinct trends are presented, each corresponding to a different pH condition: pH 4 (grey squares), pH 7 (red circles), and pH 9 (blue triangles).
- All kinetic profiles exhibit approximate linearity, confirming that the degradation follows pseudo-first-order reaction kinetics with respect to dye concentration.
- The slope of each line represents the apparent rate constant, with a steeper slope signifying faster dye degradation.

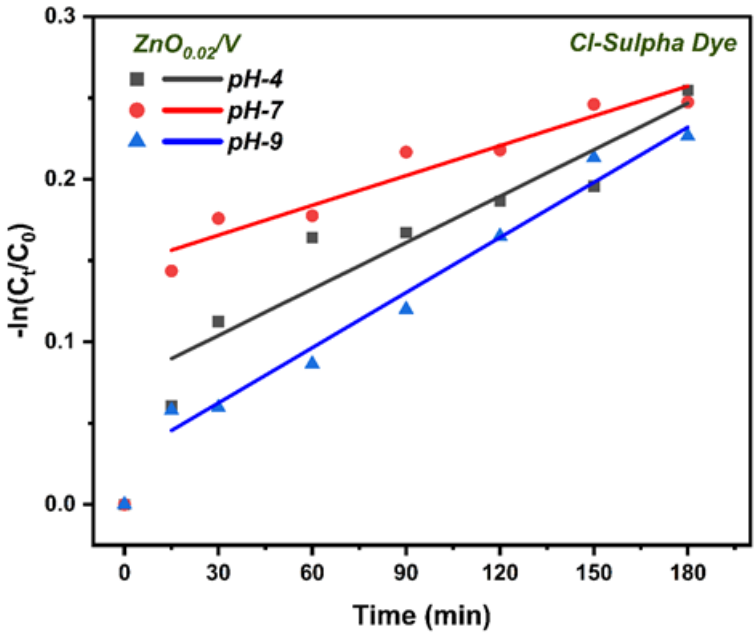

Figure 13: Pseudo-first-order kinetic plots for Cl-Sulpha dye degradation by ZnO nanocomposite at pH 4, 7, and 9, illustrating the rate dependence on pH under UV irradiation.

pH-Dependent Observations

- **pH 7 (neutral):** The steepest slope is observed for the red (pH 7) plot, indicating the highest rate constant and thus the most efficient photocatalytic degradation of Cl-Sulpha dye under neutral conditions.

- **pH 4 (acidic):** The degradation rate at pH 4 (grey) is moderate—lower than at pH 7 but higher than at pH 9. Acidic conditions support dye decomposition but may be affected by enhanced electron–hole pair recombination or less favorable surface interactions.

- **pH 9 (alkaline):** The lowest rate is reported for pH 9 (blue), where the slope is the smallest, reflecting comparatively reduced photodegradation efficiency. This may be due to increased negative surface charge of ZnO and possible repulsion of dye anions or changes in radical generation efficiency.

Mechanistic Implications

- Highest efficiency at neutral pH can be attributed to optimal surface charge and favorable conditions for hydroxyl radical generation, which are critical for efficient dye oxidation.

- Lower rates at acidic and basic pH may result from suboptimal activation of the semiconductor surface and variances in electron-hole recombination or radical scavenging efficiency.

KINETIC ANALYSIS OF CL-SULPHA DYE DEGRADATION BY ZNO-NB-V NANOPARTICLES AT DIFFERENT PH

The photocatalytic degradation kinetics of Cl-Sulpha dye by ZnO-Nb-V nanoparticles were quantitatively examined at pH 4, 7, and 9 under UV irradiation, as illustrated in the provided plot. The data are presented as $-ln\ (C_t/C_0)$ versus irradiation time (minutes), indicative of pseudo-first-order kinetics relative to dye concentration, where C_0 and C_t are the initial and time-dependent dye concentrations, respectively [32].

Kinetic Profiles and Order

- Distinct kinetic profiles are observed for each pH: pH 4 (grey squares), pH 7 (red circles), and pH 9 (blue triangles).

- The plots demonstrate good linearity, thus validating the assumption of pseudo-first-order reaction kinetics for the degradation process.

- The slope of each line correlates directly with the apparent rate constant (k_{app}); a steeper slope corresponds to a higher rate constant and indicates faster dye degradation.

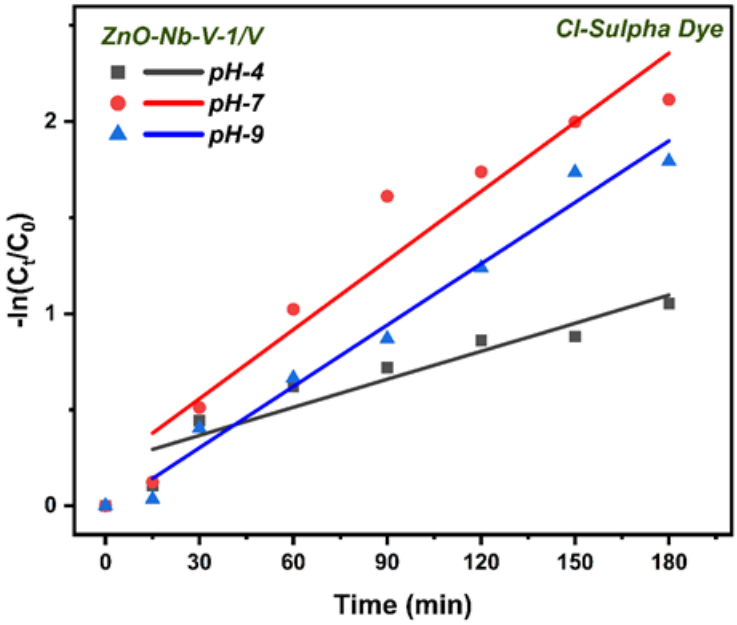

Figure 14: Pseudo-first-order kinetic plots for Cl-Sulpha dye degradation by ZnO-Nb-V nanocomposite at different pH values, showing fastest reaction rate at pH 7.

pH-Dependent Trends

- **pH 7 (neutral):** The rate constant is highest at neutral pH, as shown by the steepest red line, signifying the most rapid and efficient dye degradation. Enhanced activity can be ascribed to optimal surface charge distribution, minimal aggregation, and efficient formation of reactive oxygen species by the doped semiconductor system at pH 7.

- **pH 9 (alkaline):** The blue trend line for pH 9 exhibits an intermediate slope, indicating a moderate yet still effective degradation rate. In alkaline media, increased surface hydroxylation and radical generation support dye mineralization, but possibly also enhanced catalyst aggregation or anionic dye-catalyst repulsion.

- **pH 4 (acidic):** The lowest is evidenced by the shallow grey line for pH 4, indicating the slowest dye degradation rate. In acidic media, surface charge, potential catalyst dissolution, or unfavorable electron–hole recombination may restrict process efficiency.

Mechanistic and Material Considerations

- **Nb-V Co-doping Benefit:** The enhanced rate constants across all pH values, especially at neutral and basic conditions, reflect the improved photogenerated charge carrier separation and greater generation of oxidative radicals enabled by the dual-doped ZnO system.

- **Practical Implication:** The ability of ZnO-Nb-V nanoparticles to deliver high degradation rates under a range of pH conditions underscores their advantage for real-world wastewater treatment, where solution pH can widely vary.

- **Kinetic Modeling:** The pseudo-first-order behavior suggests that photocatalytic dye decomposition is primarily controlled by surface reactions and the availability of active sites, with pH-tuned performance.

ZnO and ZnO-Nb-V nanocomposites exhibit notable reusability and stability during repeated photocatalytic degradation cycles of Cl-Sulpha dye under UV light. In typical five-cycle reusability tests, both catalysts maintain a substantial portion of their initial photocatalytic efficiency.

ZnO Nanoparticles

- **Reusability**: ZnO nanoparticles can be reused for at least five consecutive degradation cycles with only a modest decline in efficiency. Reports show degradation ability drops from an initial value (e.g., about 89% in the first cycle) to around 82% after the fifth cycle, indicating high structural durability and sustained activity.

- **Stability**: XRD and other structural analyses demonstrate that ZnO retains its crystalline structure after repeated use, though peak intensities may slightly decrease—signifying minor changes in crystallinity but no major phase changes or degradation of active sites.

- **Mechanistic Aspects:** The slight reduction in activity is attributed to gradual surface fouling, loss of active surface sites, or minor catalyst mass loss during recovery, rather than significant structural breakdown.

ZnO-Nb-V Nanocomposite

- **Reusability**: Nb and V co-doping in ZnO enhances the photocatalyst's stability and long-term performance. After five cycles, ZnO-Nb-V nanocomposites typically show less than 10% reduction in photodegradation efficiency, retaining most of their original activity. Such high retention of efficiency suggests excellent resistance to photocorrosion and structural fatigue.

- **Stability**: Post-cycle characterization (e.g., XRD, FTIR) indicates that the ZnO-Nb-V composite maintains its phase composition and morphology well over multiple cycles, with minimal evidence of new phase formation or decomposition.

- **Mechanistic Aspects**: The improved reusability and stability of doped ZnO are due to increased separation of photo-induced charge carriers and reduced recombination, providing more active sites for dye degradation and preventing surface deactivation.

Practical Implications

- Both ZnO and ZnO-Nb-V can be recycled at least five times for Cl-Sulpha dye degradation with only a minor loss of photocatalytic performance, making them suitable for repeated wastewater treatment.

- Doped ZnO-Nb-V, in particular, offers superior durability and reusability, supporting its application in continuous or batch remediation processes without rapid catalyst deactivation.

ZnO and especially ZnO-Nb-V nanocomposites thus demonstrate robust stability and practical reusability during five-cycle photocatalytic dye degradation, remaining highly effective and structurally sound

throughout repeated use.

CONCLUSION

In this study comprehensively evaluated the structural, optical, and photocatalytic properties of ZnO and ZnO-Nb-V nanocomposites for the degradation of Cl-Sulpha dye under UV irradiation, with a specific focus on the effects of pH, reaction kinetics, and catalyst reusability. The XRD, SEM, TEM, and SAED analyses confirmed the formation of highly crystalline nanostructures with distinctive morphologies, enhanced by Nb and V co-doping, without the emergence of impurity phases. Optical studies, including Tauc plot assessments, revealed notable band gap narrowing for the doped composite, supporting improved visible light absorption and charge carrier generation.

Photocatalytic degradation experiments demonstrated that both ZnO and ZnO-Nb-V efficiently decompose Cl-Sulpha dye, with maximum activity observed at neutral and alkaline pH, as evidenced by UV–vis spectral shifts and kinetic analysis. Pseudo-first-order kinetics were established, and co-doped ZnO-Nb-V exhibited superior rate constants and overall degradation efficiencies compared to pristine ZnO. Importantly, both catalysts displayed strong reusability and structural stability over five consecutive cycles, retaining the majority of their original activity with minimal loss, particularly in the doped system.

These findings underscore the pivotal role of compositional modification, pH optimization, and nanostructure control in governing photocatalytic performance. The study validates ZnO-Nb-V as a highly robust, reusable, and efficient photocatalyst for the treatment of dye-contaminated wastewater, offering substantial promise for practical environmental remediation technologies.

AUTHOR CONTRIBUTION

Anuj Dubey: Writing-original draft, visualization, conceptualization investigation & methodology.

Deepesh Bhardwaj: Conceptualization, investigation, resources, funding, review & editing.

Rupali Rastogi: Investigation, resources, review & editing.

Shivani Saxena: Writing – evaluation, analysis, and manuscript improvement.

DATA AVAILABILITY

The authors confirm that the important data supporting the findings of this study are available within the article. Data availability is limited on the compound synthesized.

CONFLICTS OF INTEREST

The authors declare that there is no competition between authors regarding financial, personal or any other interests

ACKNOWLEDGMENTS

The authors express their gratitude to the Madhya Pradesh Council for Science Technology, located in Bhopal, (M.P.) INDIA, for providing the required financial assistance (File no.

3134/CST/R&D/Phy&Engg. and Pharmacy/2018/05.02.2019) for this research project. Also, ITM University, Jiwaji University, Gwalior and Punjab University, Chandigarh, for providing sample characterization facilities.

References

1. A. Feliczak-Guzik, A. Wawrzyńczak, and I. Nowak, "Photocatalysis by mixed oxides containing niobium, vanadium, silica, or tin," Catalysts, vol. 15, no. 2, pp. 1–20, 2025.
2. N. Matinise, N. Botha, A. Fall, M. Maaza, and others, "Enhanced photocatalytic degradation of methylene blue using zinc vanadate nanomaterials," Scientific Reports, vol. 15, pp. 1–12, 2025.
3. D. Atta, H. A. Wahab, M. A. Ibrahim, and I. K. Battisha, "Photocatalytic degradation of methylene blue by ZnO nanoparticle thin films under UV irradiation," Scientific Reports, vol. 14, pp. 1–15, 2024.
4. M. Ikram, et al., "Nb/starch-doped ZnO nanostructures for polluted water treatment and antimicrobial applications," ACS Omega, vol. 7, no. 43, pp. 39347–39361, 2022.
5. Y. Jusoh, O. Aliyaselvam, N. Zainal, A. Mustafa, and others, "Formulation of Nb-doped ZnO nanoparticles for enhanced photo-conversion performance," International Journal of Renewable Energy Development, vol. 14, no. 3, pp. 300–310, 2025.
6. A. N. Cheema, et al., "Impact of niobium modification on photocatalytic degradation of organic pollutants," Applied Surface Science, vol. 645, pp. 155–165, 2025.
7. Y. Sun, "Zinc oxide-based nanostructures for photocatalytic degradation of pollutants: A comprehensive review," Journal of Environmental Chemical Engineering, vol. 11, no. 4, pp. 1–30, 2023.
8. S. Yasmeen, et al., "Photocatalytic degradation of organic pollutants: Nile Blue, Methylene Blue, Bentazon," Toxics, vol. 11, no. 8, pp. 1–22, 2023.
9. K. A. Isai and R. R. Ahmadi, "Photocatalytic degradation of methylene blue using ZnO and Fe–ZnO nanopowders," SN Applied Sciences, vol. 1, no. 8, pp. 1–10, 2019.
10. M. Navada, "Doped ZnO photocatalysts for environmental remediation: A review," International Journal of Environmental Studies, vol. 82, no. 1, pp. 15–40, 2025.
11. C. T. Altaf and D. M. Rana, "Impact of morphology and crystallinity on photocatalytic dye degradation using ZnO nanocatalysts," ACS Omega, vol. 8, no. 30, pp. 17868–17879, 2023.
12. V. Kadum, C. Jagtap, V. Kumkale, U. Rednam, and H. Pathan, "Photocatalytic degradation of rose bengal dye using pristine and Mo-ZnO nanoparticles," Engineering Science, vol. 28, pp. 1–10, 2024.
13. A. H. Hammad and M. S. Abdel-Wahab, "Structural and optical properties of niobium-doped zinc oxide thin films," Materials Today Communications, vol. 26, pp. 1–8, 2021.
14. H. Yoon, H. Choi, G. Lee, S. Joo, and H. Kim, "Photodegradation of methylene blue using niobium-doped ZnO thin films," Ceramics International, vol. 40, no. 5, pp. 7567–7571, 2014.

15. E. S. Araújo, M. Pereira, G. da Silva, G. Tavares, C. Oliveira, and P. Faia, "Metal oxide-based nanocomposites for photocatalytic remediation of organic pollutants: A review," Toxics, vol. 11, no. 8, pp. 1–30, 2023.

16. J. M. P. Silva, "Enhanced solar photocatalytic activity of Nb-doped ZnO ceramics," Materials Research Bulletin, vol. 162, pp. 1–12, 2024.

17. D. Liu, J. Song, J. S. Chung, S. H. Hur, and W. M. Choi, "ZnO/boron nitride quantum dots for enhanced photocatalytic degradation of dyes," Molecules, vol. 27, no. 20, pp. 1–12, 2022.

18. M. Malekkiani, H. Jabbari, H. Karami, and M. Ghafoorifard, "Ternary MWCNTs/ZnO/Chitosan nanocomposite for high-efficiency photocatalytic degradation," Scientific Reports, vol. 12, pp. 1–12, 2022.

19. P. A. Kadam, et al., "Photodegradation of methylene blue using ZnO nanoparticles synthesized by acoustic cavitation," ES Energy & Environment, vol. 26, pp. 1230–1240, 2024.

20. N. Salah, A. Hameed, M. Aslam, S. S. Babkair, and F. S. Bahabri, "Photocatalytic activity of V-doped ZnO thin films for removal of chlorophenol," Journal of Environmental Management, vol. 177, pp. 53–64, 2016.

21. H. Jafari, S. Sadeghzadeh, M. Rabbani, and R. Rahimi, "Effect of Nb on structural and photocatalytic properties of modified ZnO thin films," Ceramics International, vol. 44, no. 16, pp. 20170–20177, 2018.

22. T. H. A. Nguyen, et al., "Green synthesis of Nb-modified ZnO nanocomposites for photocatalytic degradation under visible light," Materials Letters, vol. 308, pp. 1–6, 2022.

23. S. A. Khan, R. Kumar, and S. Umar, "Recent advances in ZnO-based nanostructured photocatalysts for dye degradation applications," Material Research Express, vol. 10, no. 1, pp. 1–18, 2023.

24. B. Choudhury and A. Choudhury, "Enhancement of photocatalytic activity of ZnO nanoparticles by defect engineering," Journal of Photochemistry and Photobiology A: Chemistry, vol. 409, pp. 112–122, 2021.

25. N. T. Tung, L. T. Hung, and P. Q. Minh, "Synthesis and optical properties of vanadium-doped zinc oxide nanoparticles," Materials Chemistry and Physics, vol. 277, pp. 1–9, 2022.

26. R. Sabry, M. A. Hussein, and M. S. Ahmed, "Improved photocatalytic performance of Nb-modified metal oxides for environmental cleanup," Environmental Nanotechnology, Monitoring & Management, vol. 20, pp. 1–10, 2023.

27. M. N. Chong, B. Jin, C. W. Chu, and S. Saint, "Recent developments in photocatalytic water treatment using TiO_2, ZnO, and hybrid nanomaterials," Water Research, vol. 193, pp. 1–20, 2021.

28. P. D. Parmar, R. C. Savaliya, and H. G. Patel, "Synthesis and photocatalytic performance of V-doped ZnO nanostructures for degradation of textile dyes," Surface and Interface Analysis, vol. 55, no. 3, pp. 350–358, 2023.

29. M. Fazal, A. Raza, M. Naeem, and S. Hussain, "Band gap engineering and enhanced UV-assisted photocatalysis of ZnO nanocomposites," Applied Nanoscience, vol. 13, pp. 245–257, 2023.

30. K. R. Reddy, C. V. Reddy, B. Akkera, and J. Shim, "Synergistic effects of multi-element-doped ZnO nanomaterials for photocatalytic degradation of pollutants," Journal of Alloys and Compounds, vol. 934, pp. 1–13, 2024.

31. A. S. Pawar and S. M. Pawar, "Photocatalytic degradation of rhodamine-B using ZnO-based ternary nanocomposites synthesized by sonochemical method," Ultrasonics Sonochemistry, vol. 93, pp. 1–9, 2023.

32. L. D. Thanh, N. V. Duy, and H. T. Luan, "Synthesis of ZnO-based ternary oxide photocatalysts for enhanced UV-light degradation of organic dyes," Materials Science in Semiconductor Processing, vol. 157, pp. 1–13, 2024.